Eur. J. Biochem. 265, 20–26 (1999) © FEBS 1999

Mechanism of porcine pancreatic α-amylase

Inhibition of amylose and maltopentaose hydrolysis by kidney bean (*Phaseolus vulgaris*) inhibitor and comparison with that by acarbose

Roger Koukiekolo[1], Véronique Le Berre-Anton[2], Véronique Desseaux[1], Yann Moreau[3], Pierre Rougé[2], Guy Marchis-Mouren[1] and Marius Santimone[1]

[1]*Laboratoire de Biochimie et Biologie de la Nutrition CNRS ESA 6033, Faculté des Sciences et Techniques de St Jérôme, Université d'Aix-Marseille, France,* [2]*Institut de Pharmacologie et Biologie Structurale CNRS UPR 9062, Toulouse, France,* [3]*IRD Laboratoire de Biochimie et Biologie de la Nutrition CNRS ESA 6033, Faculté des Sciences et Techniques de St Jérôme, Université d'Aix-Marseille, France*

The effects of *Phaseolus vulgaris* inhibitor (α-AI) on the amylose and maltopentaose hydrolysis catalysed by porcine pancreatic α-amylase (PPA) were investigated. Based on a statistical analysis of the kinetic data and using the general velocity equation, which is valid at equilibrium for all types of inhibition in a single-substrate reaction, it was concluded that the inhibitory mode is of the mixed noncompetitive type involving two molecules of inhibitor. In line with this conclusion, the Lineweaver–Burk primary plots intersect in the second quadrant and the secondary plots of the slopes and the intercepts versus the inhibitor concentrations are parabolic curves, whether the substrate used was amylose or maltopentaose. A specific inhibition model of the mixed noncompetitive type applies here. This model differs from those previously proposed for acarbose [Al Kazaz, M., Desseaux, V., Marchis-Mouren, G., Payan, F., Forest, E. & Santimone, M. (1996) *Eur. J. Biochem.* 241, 787–796 and Al Kazaz, M., Desseaux, V., Marchis-Mouren, G., Prodanov, E. & Santimone, M. (1998) *Eur. J. Biochem.* 252, 100–107]. In particular, with α-AI, the inhibition takes place only when PPA and α-AI are preincubated together before the substrate is added. This shows that the inhibitory PPA–αAI complex is formed during the preincubation period. Secondly, other inhibitory complexes are formed, in which two molecules of inhibitor are bound to either the free enzyme or the enzyme–substrate complex. The catalytic efficiency was determined both with and without inhibitor. Using the same molar concentration of inhibitor, α-AI was found to be a much stronger inhibitor than acarbose. However, when the inhibitor amount is expressed on a weight basis ($mg \cdot L^{-1}$), the opposite conclusion is drawn. In addition, limited proteolysis was performed on PPA alone and on the α-AI–PPA complex. The results show that, in the complex, PPA is more sensitive to subtilisin attack, and shorter fragments are obtained. These data reflect the conformational changes undergone by PPA as the result of the protein inhibitor binding, which differ from those previously observed with acarbose.

Keywords: amylose; enzyme kinetics; maltopentaose; *Phaseolus vulgaris*; α-amylase.

α-Amylases catalyse the hydrolysis of internal α-(1→4) glucosidic linkages. They are retaining glycosidases which belong to the 13 family glycoside hydrolase [1]. They are widely distributed among Archaea, Bacteria and Eucarya [2,3]. The 496-amino acid sequence of porcine pancreatic α-amylase (PPA) has been determined [4,5] and the three-dimensional structure obtained at 0.2 nm resolution [6,7]. Following the $(\beta/\alpha)_8$ barrel (residues 1–405), PPA contains a C-terminal β-stranded domain (residues 406–496) with an α-crystalline topology.

The structure of PPA complexed with acarbose, a pseudo-tetrasaccharide [8], was determined by Fourier difference analysis, and the interactions occurring at the active site were identified. An additional surface carbohydrate-binding site has been detected in the $A_{\alpha 7}A_{\alpha 8}$ region facing the C-terminal domain segment between β9 and β10 in the 4,4′-dithio-α-maltotrioside–PPA complex [6,9]. Two additional carbohydrate-binding sites have also been observed in the maltopentaose–PPA complex [10].

Kinetic studies have been carried out recently to determine the mechanism underlying the inhibitory effect of acarbose, using substrates of various lengths such as amylose [degree of polymerization (DP) 4900], maltodextrin (DP 18) and maltopentaose [11,12]. The inhibition is of the mixed noncompetitive type and either one or two molecules of acarbose bind(s) to PPA, whether the substrate is maltopentaose or amylose. The role of these two sugar-recognition sites and their link with the active site, possibly in the product processing, have not yet been elucidated.

α-AI is a lectin-like inhibitor of the animal and insect α-amylases, present in red kidney bean (*Phaseolus vulgaris*). This inhibitor is a 56-kDa dimeric glycoprotein ($\alpha_2\beta_2$) [13]. X-ray analysis of α-AI cocrystallized with PPA showed the existence of a complex at 0.18 nm resolution with a 1 : 2

Correspondence to M. Santimone, Laboratoire de Biochimie et de Biologie de la Nutrition, Av. Escadrille Normandie Niemen, case 342, F-13397 Marseille cédex 20, France. Fax: + 33 4 91 288440,
E-mail: Yann.Moreau@mpl.orstom.fr

Abbreviations: PPA, porcine pancreatic α-amylase; α-AI, α-amylase inhibitor from kidney bean (*Phaseolus vulgaris*) type I; DP, degree of polymerization.

Enzyme: retaining α-(1→4)-glucan-4-glucanohydrolase (EC 3.2.1.1).

(Received 29 January 1999, revised 9 April 1999, accepted 6 June 1999)

stoichiometry (α-AI/PPA) [14]. Two hairpin loops, extending out from the jelly roll fold of a monomer, interact directly with the active-site region of PPA, and the inhibitor molecule fills the whole substrate-docking region of the enzyme. Preliminary results obtained with the *p*-nitrophenyl-α-D-maltoside substrate analogue show that the binding of α-AI to PPA is a slow process [15]. This remarkable feature has been confirmed for PPA [13] and the human enzyme [16]; maximum inhibition is reached after 30 min in contact.

In the present paper, we describe the inhibitory effects of α-AI on the kinetics of the hydrolysis of amylose DP 4900, a long substrate, and maltopentaose, a short one, catalysed by PPA. The type of inhibition exerted by α-AI is discussed. A model is proposed that accounts for the slow binding of the inhibitor to the enzyme and for crystallographic, biochemical and physicochemical data.

Finally the inhibition process is compared with that of acarbose.

MATERIALS AND METHODS

Materials

PPA was purified from porcine pancreas [17], replacing DEAE-cellulose by Accell™ Plus QMA Anion Exchanger (Quaternary Methylamine, 50 nm) from Waters in the chromatographic separation procedure, and subsequently concentrated by ultrafiltration through a PM10 membrane (Amicon) up to 6–8 mg·mL^{-1}. The amylase concentration was determined by measuring A_{280} ($A_{280}^{1\%} = 25$) [11]. Subtilisin (subtilopeptidase A from *Bacillus subtilis*) was from Boehringer-Mannheim. Acrylamide solution (40% w/v), *N,N,N′,N′*-tetramethylenediamine and persulfate were from Pharmacia (Sweden), *N,N′*-methylenebisacrylamide was from Serva. Amylose (type III from potato) was from Sigma and the degree of polymerization, DP 4900, was determined by intrinsic viscosimetry [18]. Maltopentaose, maltotriose, neocuproin hydrochloride, Ponceau red and silver nitrate were from Sigma. The α-amylase inhibitor α-AI isolated from kidney bean (*Phaseolus vulgaris* cv Tendergreen) seeds was purified as previously described [13].

Kinetics

Kinetic experiments were performed at 30 °C in 20 mM sodium phosphate, pH 6.9, containing 6 mM NaCl and 1 mM sodium azide. Amylase was preincubated in the above medium with and without α-AI at 30 °C for 2 h when amylose was used as the substrate, and for 30 min when maltopentaose was used. The reaction was initiated by adding the substrate. More than 10 concentrations of each substrate, amylose (8.55–171 nM) and maltopentaose (25–500 μM), were used. Amylase concentration was 0.3 nM and that of α-AI was 48–70 nM for amylose and 100–500 nM for maltopentaose. Samples (100 μL) were collected at appropriate time intervals (0.25, 0.5, 0.75 and 1.00 min) and, in the case of amylose, immediately mixed with 1 mL chilled 0.38 M sodium carbonate containing 1.8 mM cupric sulfate and 0.2 M glycine, and kept on ice. The reducing power was determined by reductometry [19]. In the case of maltopentaose, the reaction was stopped with 0.1 M NaOH (300 μL) and kept on ice. Appropriate controls were performed at zero time. The concentrations of the reaction products (maltotriose and maltose) and the substrate (maltopentaose) concentration were determined by ion-exchange chromatography as described below [12]. The initial velocity was determined from the slope, calculated by linear regression, of the 0.25–1.00 min linear part of the kinetic curves giving the changes in the product concentration. All the experiments were repeated three or four times.

Statistical analysis

The GLM procedures were performed using the SAS/STAT software program [20]. Statistical tests were performed at 0.05 significance level. The resulting Lineweaver–Burk plots and replots were checked using the Cleland method [21].

Chromatographic analysis

Products of maltopentaose enzymatic hydrolysis and maltopentaose were analysed by high-performance anion-exchange chromatography coupled with a pulsed amperometric detector. The Dionex DX 500 chromatography HPLC system equipped with a GP 40 gradient pump and an ED 40 electrochemical detector was used as previously described [12].

Limited proteolysis

Samples in 50 mM Tris/HCl buffer (pH 7.4) containing 1 mM sodium azide were treated with 2% subtilisin for 24 h at 30 °C, and the digestion was stopped by adding 1 mM di-isopropyl fluorophosphate [22]. SDS/PAGE for size estimation of the fragments was performed as described by Laemmli [23]. After electrophoresis, the gel was equilibrated for 10–20 min with transfer buffer (50 mM Tris/borate, pH 8) and then electroblotted onto 0.1-μm thick Immobilon TM-PSQ (Millipore, Bedford, MA, USA). Staining was performed with either Ponceau red or silver nitrate solution.

RESULTS AND DISCUSSION

Limited proteolysis

α-AI, PPA and the incubated PPA–α-AI mixture, at the indicated PPA/α-AI ratios (see legend of Fig. 1), were treated with 2% subtilisin for 24 h at 30 °C. The digested samples were analysed by SDS/PAGE. α-AI and α-AI–subtilisin treated samples give similar patterns: two groups of bands, one at about 30 kDa and the other at about 15 kDa (Fig. 1, lane 7). This 15-kDa region is rather broad because of heterogeneous glycosylation [13]. This shows that under our conditions α-AI

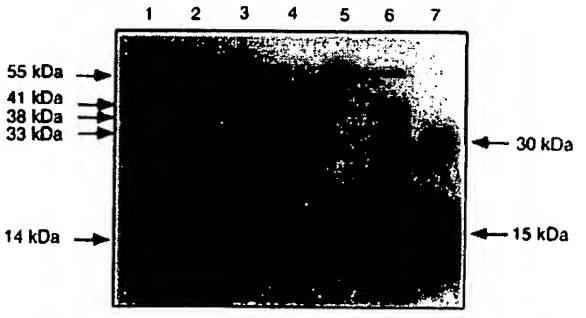

Fig. 1. SDS/PAGE analysis. PPA (lane1), PPA–subtilisin 2% (lane 2), α-AI (lane 7), PPA–α-AI at an α-AI/PPA ratio of 1 (lane 5), PPA–α-AI–subtilisin 2% with an α-AI/PPA ratio of 0.4 (lane 3), 1 (lane 4) and 10 (lane 6). Loading: 1.5 μg protein per well. The molecular masses indicated on each side come from protein marker migration (not shown).

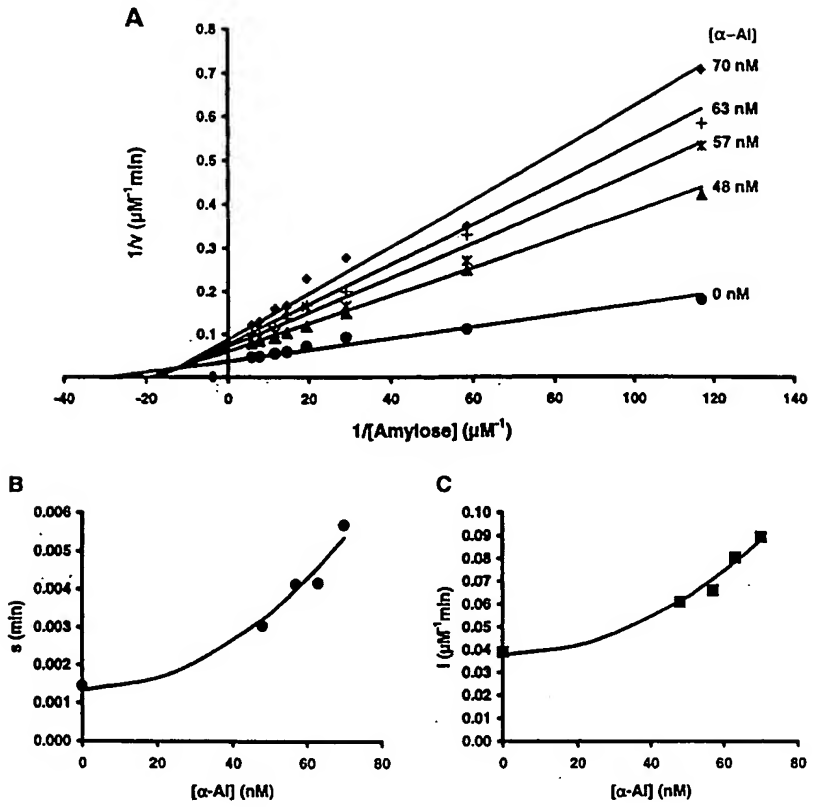

Fig. 2. Lineweaver–Burk plot using amylose as substrate. (A) Reciprocal plots obtained with variable amylose concentrations and at fixed concentration of the *Phaseolus* inhibitor α-AI. The reciprocal plots are drawn from one set of data. (B, C) Secondary plots showing the dependence of the vertical axis intercept (*i*) and of the slope (*s*) on the concentration of *Phaseolus* inhibitor α-AI.

does not undergo subtilisin attack. PPA control (lane 1) migrates as a single band at 55 kDa. After subtilisin digestion, about half of the PPA is cleaved into 41-kDa and 14-kDa fragments (lane 2), as observed previously in our laboratory [22].

When the α-AI–PPA complex was digested with subtilisin at 0.4 (lane 3), 1 (lane 4) and 10 (lane 6) α-AI/PPA ratio, almost complete hydrolysis of PPA occurs and all three bands were present (38, 33 and 14 kDa). Therefore, whatever the α-AI/PPA ratio, the 41-kDa fragment is not present and more complete digestion of PPA in the PPA–α-AI complex is obtained. Sequence analysis of the 38-kDa and 33-kDa fragments at their N-terminal sequence yielded T6, Q7, S8, G9, R10 and T11. These fragments therefore both originate from the 41-kDa component. Five residues were removed from the N-terminal pyroGlu end. These fragments were also shorter at the C-terminus than the 41-kDa compound. These results show that PPA is much more sensitive to subtilisin attack in the inhibitor–enzyme complex, which suggests that the conformation of PPA changes when complexed. A change in the three-dimensional structure has in fact been detected by Fourier difference analysis [14].

Kinetics

As reported previously [13], no immediate inhibition was observed when substrate, PPA and α-AI were mixed together. PPA has to be preincubated with α-AI before the substrate is added to the reaction mixture. A prolonged preincubation period at 30 °C of 2 h for amylose and 30 min for maltopentaose was adopted. The prolonged incubation period ensures that complete equilibrium is reached between the enzyme, the inhibitor and the enzyme–inhibitor complex and allows us to postulate that the mechanism is at equilibrium. This assumption fits with experimental results: all the Lineweaver–Burk plots obtained were linear (Figs 2A and 3A).

The inhibition by α-AI of the amylose DP 4900 (a long-chain substrate) and maltopentaose DP 5 (a short-chain substrate) hydrolysis catalysed by amylase was studied in parallel.

Statistical analysis of kinetic data

Whatever the type of inhibition involved (competitive, uncompetitive or noncompetitive) and assuming the rapid equilibrium hypothesis, the initial velocity fits the following general equation:

$$v_i = \frac{C[S]}{A_0 + B_0[S] + B_1[S][I] + A_1[I]} \quad (1)$$

where A_0, A_1, B_0, B_1 and C are parameters depending on equilibrium constants and [S] and [I] are the substrate and inhibitor concentrations, respectively.

This equation is valid when one molecule of I is involved. When the inhibition is noncompetitive, A_1 and B_1 are positive. If $B_1 = 0$, the inhibition is competitive, whereas if $A_1 = 0$, the inhibition is of the uncompetitive type.

When two molecules of inhibitor are involved in the binding process with either the enzyme and/or the enzyme–substrate complex, the denominator is a second-order polynome with respect to [I]. In this case, the equation obtained can be rewritten as [24]:

$$\frac{[S]}{v} = a_0 + a_1[I] + a_2[I]^2 + [S](b_0 + b_1[I] + b_2[I]^2) \quad (2)$$

Table 1. Polynomial regression analysis of the kinetic data. The coefficients are from Eqn (2). DF, degree of freedom; *F*, Fisher statistical significance (type III) with the probability *P* of finding an *F* value greater than the calculated ones.

Substrate	Coefficient	DF	*P>F*
Amylose	b_0	34	0.0001
	b_1	34	0.4735
	b_2	34	0.0104
	a_1	34	0.4779
	a_2	34	0.0164
Maltopentaose	b_0	78	0.0001
	b_1	78	0.0885
	b_2	78	0.0001
	a_1	78	0.4790
	a_2	78	0.0001

where a_0, a_1, a_2, b_0, b_1 and b_2 are coefficients depending on the equilibrium constants.

It should be pointed out that the [S]/*v* equation (Eqn 2) is linear with respect to [S] at fixed I concentration at rapid equilibrium; in the steady state, the initial velocity calculated by the King and Altman method [25] also gives a linear [S]/*v* versus [S] equation except with a model of random type [11].

The data were adjusted to Eqn (2) by performing a polynomial regression analysis which makes it possible to test whether or not coefficients a_1, a_2, b_0, b_1 and b_2 are significant. Note that coefficients a_1, a_2 and b_1, b_2 correspond to the presence of EI, EI_2 and ESI, ESI_2 enzyme species in the reaction mixture. The results of this analysis are summarized in Table 1. With both substrates (amylose and maltopentaose), only coefficients b_0, b_2 and a_2 differed significantly from zero, while coefficients b_1 and a_1 did not.

EI_2 and ESI_2 were therefore present in the reaction medium in significant concentrations, while EI and ESI were probably present in very low concentrations. In other words two inhibitor molecules were found to have bound to both the free enzyme and the enzyme–substrate complex.

Lineweaver–Burk plots and replots

Eqn (2) can be rewritten as follows:

$$\frac{1}{v} = (a_0 + a_1[I] + a_2[I]^2)\frac{1}{[S]} + b_0 + b_1[I] + b_2[I]^2 \quad (3)$$

Lineweaver–Burk plots and the corresponding secondary plots fit this equation (Figs 2 and 3). The primary plots of the inhibition of amylose (Fig. 2A) and maltopentaose (Fig. 3A) hydrolysis were quite similar. Straight lines were obtained with each substrate. Both the slope *s* and the vertical axis intercept *i* increased with increasing *Phaseolus* inhibitor concentrations [I]. As was to be expected, the analysis of these results by the Cleland method [21] accounts for noncompetitive inhibition. In addition, it is worth noting that, in the primary plots, the intercepts were in the second quadrant. The inhibition was therefore of the mixed noncompetitive kind.

As in competitive inhibition, the effects of the α-AI concentration, [I], on the slope indicate that I binds to the free enzyme E, while the effects of the α-AI concentration on the vertical axis intercept show that I binds to the enzyme–substrate complex ES, as in uncompetitive inhibition.

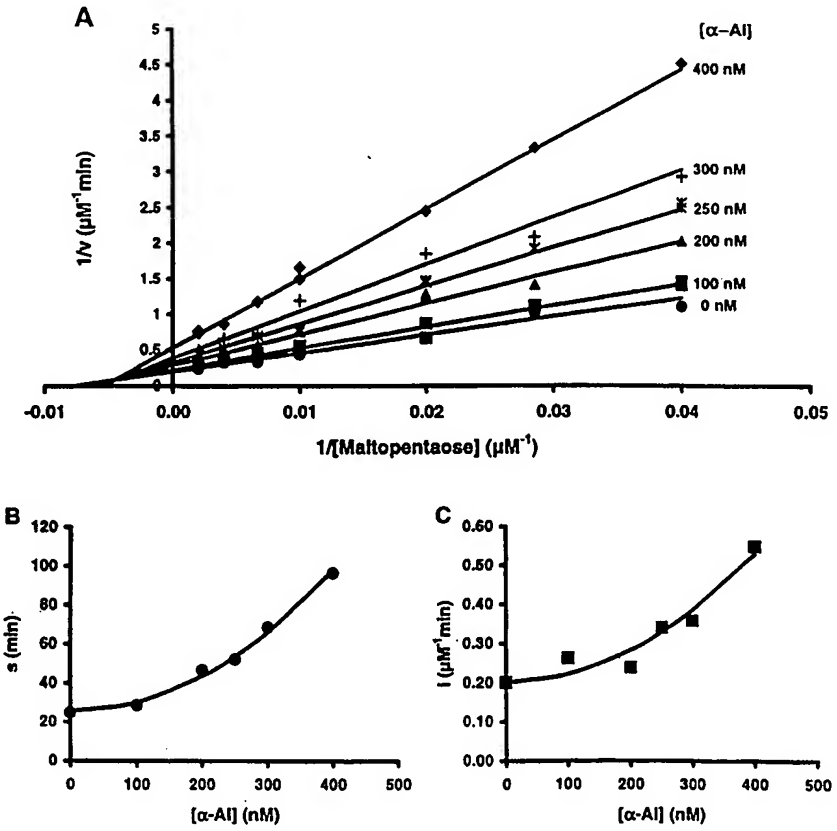

Fig. 3. Lineweaver–Burk plot using maltopentaose as substrate. (A) Reciprocal plots obtained with variable maltopentaose concentrations and at fixed concentration of the *Phaseolus* inhibitor α-AI. The reciprocal plots are drawn from one set of data. (B, C) Secondary plots showing the dependence of the vertical axis intercept (*i*) and of the slope (*s*) on the concentration of *Phaseolus* inhibitor α-AI.

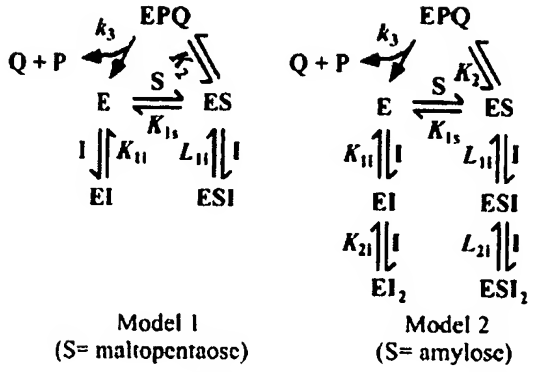

Fig. 4. Two models proposed for the noncompetitive inhibition of PPA-catalysed amylose (model 1) and maltopentaose (model 2) hydrolysis. P and Q are products. K and L are dissociation equlibrium constants and k_3 a rate constant.

The secondary Lineweaver–Burk plots of the amylose (Fig. 2B,C) and maltopentaose hydrolysis (Fig. 3B,C) were also similar: plotting both the slope s and the vertical axis intercept i against the inhibitor concentration produced parabolic lines. The respective second-order equations of these lines with respect to inhibitor concentration [I] are consistent with the results of the above statistical analysis: two I molecules bind to both the free enzyme and the enzyme–substrate complex.

Comparison between α-AI and acarbose inhibition: kinetics and model

The inhibitory effects on PPA-catalysed amylose and maltopentaose hydrolysis were previously studied at our laboratory using pseudotetrasaccharide acarbose as the inhibitor [11,12]. Lineweaver–Burk plots were analysed using the Cleland method [21]: the effects of the inhibitor concentration on the slope and on the vertical axis intercept of the primary plots were studied. Inhibition was found to be of the noncompetitive type involving either one or two molecules of inhibitor, whether the substrate was maltopentaose or amylose. Two models (1 and 2) were proposed involving abortive complexes (Fig. 4).

Do these models fit the data obtained in the case of *P. vulgaris* inhibition? Model 1 has to be ruled out because only one I molecule binds to both the enzyme E and the enzyme–substrate complex ES. Model 2 agrees with the statistical analysis of the *Phaseolus* inhibition, as two I molecules bind to both the free enzyme E and the enzyme complex ES as complexes EI_2 and ESI_2, respectively. However, this model predicts that inhibition will occur without any preincubation of the inhibitor with the enzyme. When the enzyme is actually added to the reaction mixture containing the substrate (amylose/maltopentaose) and the *Phaseolus* inhibitor, no inhibition occurs at first: the inhibitor concentration has no effect on the slope or on the vertical axis intercept of the primary plots. Inhibition is observed only when the enzyme and the inhibitor have been initially preincubated for at least 10 min before addition of the substrate. This suggests that neither EI nor the ESI complex is present in detectable amounts at the beginning of the reaction and consequently that both reactions:

$$E + I \underset{k_{-1}}{\overset{k_1}{\rightleftarrows}} EI \text{ and } ES + I \underset{l_{-1}}{\overset{l_1}{\rightleftarrows}} ESI$$

are slow reactions with low rate constants, k_1 and l_1, respectively. It was previously reported in fact that EI formation

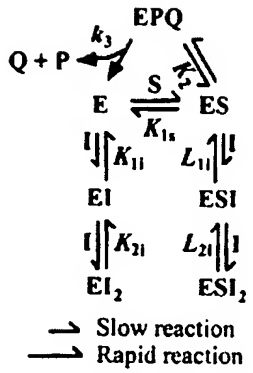

Fig. 5. Model 2′.

is a slow process [13,15]. When the inhibitor is not preincubated with the enzyme, because the formation of EI and ESI is slow, these complexes are not formed when the initial velocity is measured, therefore no immediate inhibition might be observed. Therefore, model 2′ may be valid if it is assumed that the I binding at E or ES is a slow reaction (Fig. 5).

Is this model still valid when E and I are preincubated? When E and I are preincubated, the complex EI is already formed when the substrate is added to the medium, and the inhibitory effect on the slope is observed as predicted by this model. Also, upon addition of the substrate to the reaction medium, the complex ES is immediately formed and the hydrolysis begins immediately, while the binding of I to ES is slow and the amount of ESI complex produced is likely to be very small and have no effect on the vertical axis intercept: this contradicts the data obtained here by measuring the initial velocity as the effect on the vertical axis intercept is observed. Therefore model 2′ cannot be retained.

To account for the immediate effect observed on the vertical axis intercept upon adding the substrate to the preincubated reaction medium containing E and I, one has to assume that the ESI complex is not produced by binding of I to the ES complex but that it is obtained via a different pathway, in which the inhibitor binds slowly to the enzyme before the rapid substrate binding to the EI complex occurs, giving ESI:

$$E \overset{I}{\rightleftarrows} EI \overset{S}{\rightleftarrows} EIS$$

In line with the last hypothesis, we propose model 3 (Fig. 6).

The inhibition mechanism can actually be further described on the basis of X-ray-diffraction data on the inhibitor–PPA complexes. In the crystal structure of the complex, the inhibitor I binds to two E molecules forming a single E_2I complex and

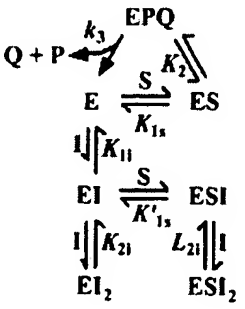

Fig. 6. Model 3.

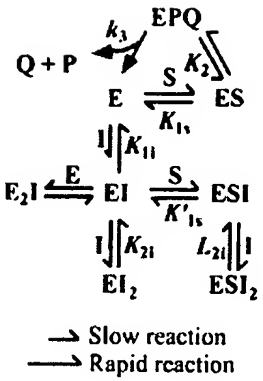

Fig. 7. Model 4.

occupies the active sites [14]. Also the results of studies using gel-filtration and light-scattering techniques applied to the analysis of the E + I preincubated mixture allow the characterization of two complexes, E_2I and EI [26]. The results obtained by the above authors diverge from each other and from the kinetics results because of the [I]/[E] ratio used: both EI and E_2I complexes were observed by Kasahara *et al.* [26] at an [I]/[E] ratio of 2, while only the E_2I complex was observed by Bompard-Gilles *et al.* [14] at a still lower ratio of 1. The two complexes EI_2 and ESI_2, in which two molecules of I are bound to the enzyme, were both observed in our kinetic experiments probably because the ratio used was much higher (160–233 when amylose was used as the substrate and 100–400 with maltopentaose).

The general model (model 4) depicted in Fig. 7 takes both our kinetic results and the crystallographic and gel-filtration data into account. In particular, this model explains how two different complexes (EI_2 and E_2I) can be obtained from the same initial complex EI. When a high E concentration is used (low [I]/[E] ratio), the equilibrium is displaced towards the formation of E_2I, whereas when a high I concentration is used (high [I]/[E] ratio), the equilibrium is displaced towards the formation of EI_2.

Comparisons between the α-AI inhibitory mechanism and that previously proposed for acarbose help us to understand the respective processes. The main difference between the acarbose scheme and that for α-AI is that the ternary complex ESI is obtained via two different pathways. In the α-AI scheme (model 4), one molecule of I binds slowly at the E active site to give EI which then accepts one S molecule at an additional site to give E–S–α-AI (ESI). Conversely, in the acarbose scheme (model 2), one molecule of S is bound at the E active site to give the ES binary complex, then one molecule of I can bind to this complex to give the E–S–acarbose (ESI) ternary complex. It should be pointed out that, in the acarbose scheme, S occupies the E active site in the ESI complex, while acarbose is bound at an additional carbohydrate-binding site, whereas, in the α-AI scheme, I occupies the E active site while S is bound at an additional site. These differences in the mechanism of PPA inhibition probably depend on the chemical type and the size of the inhibitor molecule. In fact, acarbose has no effect on the sensitivity of PPA to subtilisin in the PPA–acarbose complex (results not shown), whereas in the PPA–α-AI complex, higher sensitivity of PPA to subtilisin attack is observed. Such behaviour may originate from conformational changes. The binding of acarbose to PPA only results in a very small and discrete conformational change [27] whereas the binding of α-AI to PPA results in very large conformational changes [14] and the subtilisin sensitivity to PPA is enhanced (our results).

Lastly the inhibitory efficiencies of α-AI and acarbose were compared. As shown in Table 2, when amylose is substrate, about the same inhibition (71–74%) as assessed by catalytic efficiency is reached for 0.06 μM α-AI and 0.60 μM acarbose. Therefore, α-AI is a more efficient inhibitor of PPA than acarbose. A similar conclusion is drawn from maltopentaose hydrolysis inhibition (Table 2). Conversely, as the molecular mass of the bean inhibitor is much higher than that of acarbose, the opposite result is obtained when the inhibitor concentrations are expressed as $mg \cdot L^{-1}$. When amylose is the substrate, about the same inhibition (71–74%) as assessed by catalytic efficiency is reached for 2.70 $mg \cdot L^{-1}$ α-AI and 0.40 $mg \cdot L^{-1}$ acarbose (Table 2). A similar observation was made when maltopentaose was used as substrate. This way of expressing the inhibitor concentration should be used for pharmaceutical purposes. The same conclusions are drawn when the efficiencies of the two inhibitors assessed by catalytic constant are compared (Table 3).

Table 2. Comparison between the inhibitory efficiency of α-AI and acarbose: effect of the inhibitor concentration on catalytic efficiencies obtained with amylose or maltopentaose as substrate. The concentrations of inhibitors are given in both $\mu mol \cdot L^{-1}$ and $mg \cdot L^{-1}$. For easier comparison with respect to the substrate, concentrations are expressed in $mg \cdot L^{-1}$.

Substrate	Inhibitor	Conc. of inhibitor		k_{cat}/Km	Inhibition
		μM	$mg \cdot L^{-1}$	$(s^{-1} \cdot mg^{-1} \cdot L)$	(%)
Amylose	No	0	0	62	0
	Acarbose	0.60	0.4	18	71
	α-AI	0.06	2.7	16	74
Malto-pentaose	No	0	0	0.83	0
	Acarbose	3.00	1.9	0.42	49
	α-AI	0.25	10.7	0.36	57

Table 3. Comparison between the inhibitory efficiency of α-AI and acarbose: effect of the inhibitor concentration on the catalytic constant obtained with amylose or maltopentaose as substrate. The concentrations of inhibitors are given in both $\mu mol \cdot L^{-1}$ and $mg \cdot L^{-1}$. For easier comparison with respect to the substrate, concentrations are expressed in $mg \cdot L^{-1}$.

Substrate	Inhibitor	Conc. of inhibitor		$10^3 k_{cat}$	Inhibition
		μM	$mg\ L^{-1}$	(s^{-1})	(%)
Amylose	No	0	0	1.20	0
	Acarbose	0.60	0.4	0.62	48
	α-AI	0.06	2.7	0.69	43
Malto-pentaose	No	0	0	0.081	0
	Acarbose	0.75	0.5	0.035	57
	α-AI	0.40	17.2	0.033	59

ACKNOWLEDGEMENTS

We are very grateful to Mr C. Villard for excellent technical assistance and to Mr J. Bonicel (CNRS, Marseille, France) for peptide sequencing.

We acknowledge Professor E. Prodanov, Departmento de Bioquimica, Facultad de Medicina, Montevideo, Uruguay, for helpful advice. This work had financial support from the CEE-grant CI1-CT94-0034 and from ECOS Action no U93E04.

REFERENCES

1. McCarter, J.D. & Withers, S.G. (1994) Mechanisms of enzymatic glycoside hydrolysis. *Curr. Opin. Struct. Biol.* 4, 885–892.
2. Jespersen, H.M., MacGregor, E.A., Sierks, M.R. & Svensson, B. (1991) Comparison of the domain-level organization of starch hydrolases and related enzymes. *Biochem. J.* 280, 51–55.
3. Janecek, S. (1994) Sequence similarities and evolutionary relationships of microbial, plant and animal alpha-amylases. *Eur. J. Biochem.* 224, 519–524.
4. Pasero, L., Mazei-Pierron, Y., Abadie, B., Chicheportiche, Y. & Marchis-Mouren, G. (1986) Complete amino acid sequence and location of the 5 disulfide bridges in porcine pancreatic α-amylase. *Biochim. Biophys. Acta* 869, 147–157.
5. Darnis, S., Juge, N., Guo, X.J., Marchis-Mouren, G., Payan, F., Puigserver, A. & Chaix, J.C. (1999) Porcine pancreatic α-amylase: molecular cloning, primary structure, functional aspects. *Biochim. Biophys. Acta* (in press).
6. Buisson, G., Duée, E., Haser, R. & Payan, F. (1987) Three-dimensional structure of porcine pancreatic α-amylase at 2,9 Å resolution. Role of calcium in structure and activity. *EMBO J.* 6, 3909–3916.
7. Qian, M., Haser, R. & Payan, F. (1993) Structure and molecular model refinement of pig pancreatic α-amylase at 2.1 Å resolution. *J. Mol. Biol.* 231, 785–799.
8. Gilles, C., Astier, J.-P., Marchis-Mouren, G., Cambillau, C. & Payan, F. (1996) Crystal structure of pig pancreatic α-amylase isoenzyme II, in complex with the carbohydrate inhibitor acarbose. *Eur. J. Biochem.* 238, 561–569.
9. Qian, M., Spinelli, S., Driguez, H. & Payan, F. (1997) Structure of a pancreatic α-amylase bound to a substrate analogue at 2.03 Å resolution. *Protein Sci.* 6, 2285–2296.
10. Qian, M., Haser, R. & Payan, F. (1995) Carbohydrate binding sites in a pancreatic α-amylase-substrate complex, derived from X-ray structure analysis at 2.1 Å resolution. *Protein Sci.* 4, 747–755.
11. Al Kazaz, M., Desseaux, V., Marchis-Mouren, G., Payan, F., Forest, E. & Santimone, M. (1996) The mechanism of porcine pancreatic α-amylase. Kinetic evidence for two additional carbohydrate-binding sites. *Eur. J. Biochem.* 241, 787–796.
12. Al Kazaz, M., Desseaux, V., Marchis-Mouren, G., Prodanov, E. & Santimone, M. (1998) The mechanism of porcine pancreatic α-amylase. Inhibition of maltopentaose hydrolysis by acarbose, maltose and maltotriose. *Eur. J. Biochem.* 252, 100–107.
13. Le Berre-Anton, V., Bompard-Gilles, C., Payan, F. & Rougé, P. (1997) Characterization and functional properties of the α-amylase inhibitor (α-AI) from kidney bean (*Phaseolus vulgaris*) seeds. *Biochim. Biophys. Acta* 1343, 31–40.
14. Bompard-Gilles, C., Rousseau, P., Rougé, P. & Payan, F. (1996) Substrate mimicry in the active center of a mammalian α-amylase: structural analysis of an enzyme-inhibitor complex. *Structure* 4, 1441–1452.
15. Wilcox, E.R. & Whitaker, J.R. (1984) Some aspects of mechanism of red kidney bean a-amylase inhibitor and α-amylase. *Biochemistry* 23, 1783–1791.
16. Le Berre-Anton, V., Nahoum, V., Santimone, M., Barre, A., Marchis-Mouren, G., Payan, F. & Rougé, P. (1998) Interaction of the bean (*Phaseolus vulgaris*) α-amylase inhibitors with human α-amylases: structural and functional aspects. In *Recent Advances of Research on Antinutritional Factors in Legume Seeds and Rapeseed* (Jansman, A.J.M., Hill, G.D. & Van Der Poel, A.F.B., eds), Vol. 93, pp. 131–135. Wageningen Press, Wageningen, the Netherlands.
17. Granger, M., Abadie, B., Mazzei, Y. & Marchis-Mouren, G. (1975) Enzymatic activity of TNB blocked porcine pancreatic α-amylase. *FEBS Lett.* 50, 276–278.
18. Chen, Y., Fringant, C. & Rinaudo, M. (1997) Molecular characterization of starch by SEC: dependence of the performances on the amylopectin content. *Carbohydr. Polymer.* 33, 73–78.
19. Dygert, S., Li, L.H., Don Florida, R. & Thoma, J.A. (1965) Determination of reducing sugar with improved precision. *Anal. Chem.* 13, 367–374.
20. Sas Institute Inc. (1989) *SAS/STAT Users Guide*, v 6, 4th edn, Vol. 1, p. 943. Sas Institute Inc., Cary, NC.
21. Cleland, W.W. (1963) The kinetics of enzyme catalysed reactions with two or more substrates or products. *Biochim. Biophys. Acta* 67, 173–196.
22. Desseaux, V., Payan, F., Ajandouz, E.H., Svensson, B., Haser, R. & Marchis-Mouren, G. (1991) Effect of limited proteolysis in 8th loop of the barrel and of antibodies on porcine pancreas amylase activity. *Biochim. Biophys. Acta* 1080, 237–244.
23. Laemmli, U.K. (1970) Cleavage of structural proteins during the assembly of the head of bacteriophage T4. *Nature (London)* 227, 680–685.
24. Cornish-Bowden, A. (1995) *Analysis of Enzyme Kinetic Data*. Oxford University Press, Oxford.
25. King, E.L. & Altman, C. (1956) A schematic method of deriving the rate laws for enzyme catalyzed reactions. *J. Phys. Chem.* 60, 1375–1378.
26. Kasahara, K., Hayashi, K., Arakawa, T., Philo, J.S., Wen, J., Hara, S. & Yamaguchi, H. (1996) Complete sequence, subunit structure, and complexes with pancreatic a-amylase of an a-amylase inhibitor from *Phaseolus vulgaris* white kidney beans. *J. Biochem. (Tokyo)* 120, 177–183.
27. Qian, M., Haser, R., Buisson, G., Duee, E. & Payan, F. (1994) The active center of mammalian alpha-amylase. Structure of the complex of a pancreatic alpha-amylase with a carbohydrate inhibitor refined to 2.2-A resolution. *Biochemistry* 24, 6284–6294.